ADVANCED MATERIALS

www.advmat.de

1 cm^2 Organic Photovoltaic Cells for Indoor Application with over 20% Efficiency

Yong Cui, Huifeng Yao, Tao Zhang, Ling Hong, Bowei Gao, Kaihu Xian, Jinzhao Qin, and Jianhui Hou**

Organic photovoltaic (OPV) technologies have the advantages of fabricating larger-area and light-weight solar panels on flexible substrates by low-cost roll-to-toll production. Recently, OPV cells have achieved many significant advances with power conversion efficiency (PCE) increasing rapidly. However, large-scale solar farms using OPV modules still face great challenges, such as device stability. Herein, the applications of OPV cells in indoor light environments are studied. Via optimizing the active layers to have a good match with the indoor light source, 1 cm^2 OPV cells are fabricated and a top PCE of 22% under 1000 lux light-emitting diode (2700 K) illumination is demonstrated. In this work, the light intensities are measured carefully. Incorporated with the external quantum efficiency and photon flux spectrum, the integral current densities of the cells are calculated to confirm the reliability of the photovoltaic measurement. In addition, the devices show much better stability under continuous indoor light illumination. The results suggest that designing wide-bandgap active materials to meet the requirements for the indoor OPV cells has a great potential in achieving higher photovoltaic performance.

Organic photovoltaic (OPV) cells possess the merits of color,[1,2] transparency,[3,4] and light weight.[5,6] Over the last 3 decades, OPV cells have achieved rapid progress with the development of organic photovoltaic materials,[7–12] device structure engineering,[13–15] and understanding of device physics.[16–18] The power conversion efficiencies (PCEs) of OPV cells under 1 sun illumination have recently surpassed 16%.[19,20] However, in comparison with the competing photovoltaic technologies, such as traditional *c*-Si and newly emerging perovskite solar cells, the PCEs and lifetimes of OPV cells still need further improvement.[21] At present, grid-connected power farms or rooftop-integrated systems using OPV modules face great challenges. Nonetheless, as the OPV materials have great tunability of their absorption spectra, it is very easy to match them with varied indoor light sources, offering unique integration prospects as energy sources for off-grid indoor electronic devices.

For indoor applications, the request of high-performance OPV cells is different with that under 1 sun illumination. On the one hand, the solar radiation spectrum on earth covers the ultraviolet, visible, and infrared regions, while indoor light sources like fluorescent lamps (FLs) and light-emitting diodes (LEDs) only emit visible light ranging from 400 to 750 nm (**Figure 1**).[22] In previous reports, researchers focused on designing low-bandgap OPV materials to absorb as much as solar photons, with state-of-the-art photoactive layers with absorption edges around 800 nm.[23] For example, we used the wide-bandgap polymer PBDB-TF as a donor and low-bandgap IT-4F as an acceptor to fabricate the OPV devices,[24] where solar photons in the range from 300 to 800 nm could be effectively converted to electrons under 1 sun illuminations. When bringing these OPV cells to the indoor environment, the absorption spectra from 700 to 800 nm are redundant and, worse, lead to photovoltage losses (V_{loss}s). Therefore, for indoor applications, OPV cells should use wide-bandgap materials to make full use of these photons while maintaining high photovoltage. On the other hand, indoor light sources have considerably weaker intensities (<1 mW cm^{-2}) than 1 sun illumination (AM 1.5 G, 100 mW cm^{-2}), which leads to low charge carrier density in indoor OPV cells. Therefore, the Shockley–Read–Hall recombination resulting from trap states will be clearly observed,[25,26] where the device performance becomes highly dependent on the light intensity.[27] Therefore, the suppression of trap-mediated charge recombination is of great importance to reduce the V_{loss} for indoor applications.

In this work, light intensities are measured carefully. 1 cm^2 OPV cells were fabricated and recorded over 20% PCE in an indoor light environment. A wide-bandgap photoactive layer was used, consisting of a polymer donor PBDB-TF and a nonfullerene acceptor 3,9-bis(4-(1,1-dicyanomethylene)-3-methylene-2-oxo-cyclopenta[*b*]thiophen)-5,5,11,11-tetrakis(4-hexylphenyl)-dithieno[2,3-*d*′:2,3-*d*′]-s-indaceno[1,2-*b*:5,6-*b*′]-dithiophene (ITCC), to absorb the LED light. Under 1000 lux

Dr. Y. Cui, Dr. H. Yao, T. Zhang, L. Hong, B. Gao, K. Xian, J. Qin, Prof. J. Hou
State Key Laboratory of Polymer Physics and Chemistry
Beijing National Laboratory for Molecular Sciences
CAS Research/Education Center for Excellence in Molecular Sciences
Institute of Chemistry
Chinese Academy of Sciences
Beijing 100190, China
E-mail: yaohf@iccas.ac.cn; hjhzlz@iccas.ac.cn
L. Hong, B. Gao, K. Xian, J. Qin, Prof. J. Hou
University of Chinese Academy of Sciences
Beijing 100049, P. R. China
The ORCID identification number(s) for the author(s) of this article can be found under https://doi.org/10.1002/adma.201904512.

DOI: 10.1002/adma.201904512

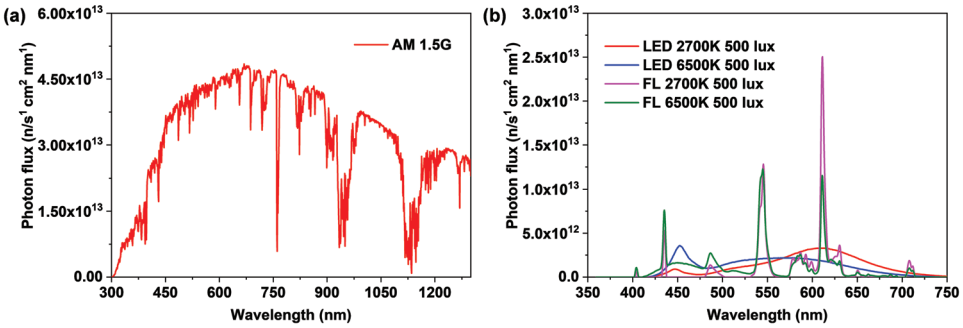

Figure 1. a) The standard AM 1.5 G solar spectrum. b) The radiative spectra of indoor light sources used in this work.

(2700 K) LED illumination, the OPV cell achieved an impressive PCE of 22.0% with an open-circuit voltage (V_{OC}) of 0.962 V, a short-circuit current density (J_{SC}) of 95.8 μA cm^{-2}, and a fill factor (FF) of 0.722. Incorporating with the EQE and photon flux spectrum, the integral current densities of the cells are calculated to be 95.2 μA cm^{-2}, confirming the reliability of photovoltaic measurement. The best device shows very good stability under continuous illumination after 500 h with over 95% of the original PCE maintained. We also studied the applications of fullerene derivative acceptor $PC_{71}BM$ and the low-bandgap nonfullerene acceptor IT-4F in the indoor OPV cells, which show relatively larger V_{loss}s and, thus, lower PCEs. Our results suggest that OPV cells have good indoor applications and match the absorption spectra with indoor light sources and low V_{loss}s are the key factors to achieve excellent photovoltaic performance.

Figure 2a shows the chemical molecular structures of the photovoltaic active materials; their molecular energy levels and absorption spectra are displayed in Figure 2. The polymer PBDB-TF is an electron donor and has demonstrated good performance when combined with both fullerene and nonfullerene acceptors in OPV cells.[28,29] The absorption of PBDB-TF covers the visible range of 300–680 nm (Figure 2b; the absorption of the blend films is shown in Figure 2c), which matches well with the LED radiative spectrum. The low-lying ionization potential of 5.47 eV ensures the higher V_{OC} in OPV cells (Figure 2d). The main absorption of $PC_{71}BM$ is located at the UV–vis region below 700 nm, making the blend film of PBDB-TF:$PC_{71}BM$ overlap the LED and FL radiative spectrum very well. However, the relatively large electron affinity (EA) of $PC_{71}BM$ implies a low V_{OC} and a large V_{loss}s in the OPV cell.

IT-4F[24] is a low-bandgap nonfullerene acceptor with an absorption onset at around 800 nm. Some works have demonstrated that the combination of PBDB-TF:IT-4F could record over 13% PCEs in OPV cells under AM 1.5 G illumination. However, when this OPV cell is transferred to an indoor light environment, the redundant absorption from 700 to 800 nm will not contribute to the J_{SC} and, on the contrary, will result in a larger V_{loss} due to its low bandgap. ITCC[30] is the other nonfullerene acceptor with a similar chemical structure to IT-4F, where the electron-withdrawing properties of fluorinated benzene in IT-4F are replaced by relatively electron-donating

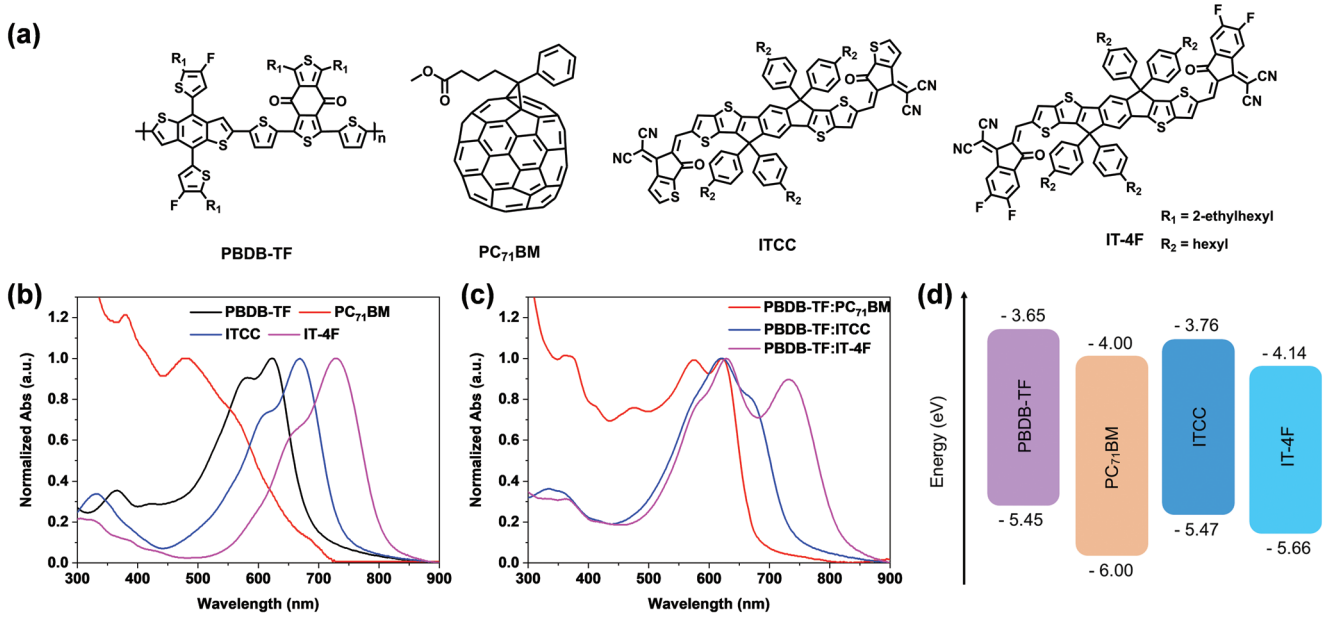

Figure 2. a) Chemical molecular structures of the polymer donor and fullerene and nonfullerene acceptors. b,c) Normalized absorption spectra of the neat films (b) and their blend films (c). d) The molecular energy level diagram of the donor and acceptors.

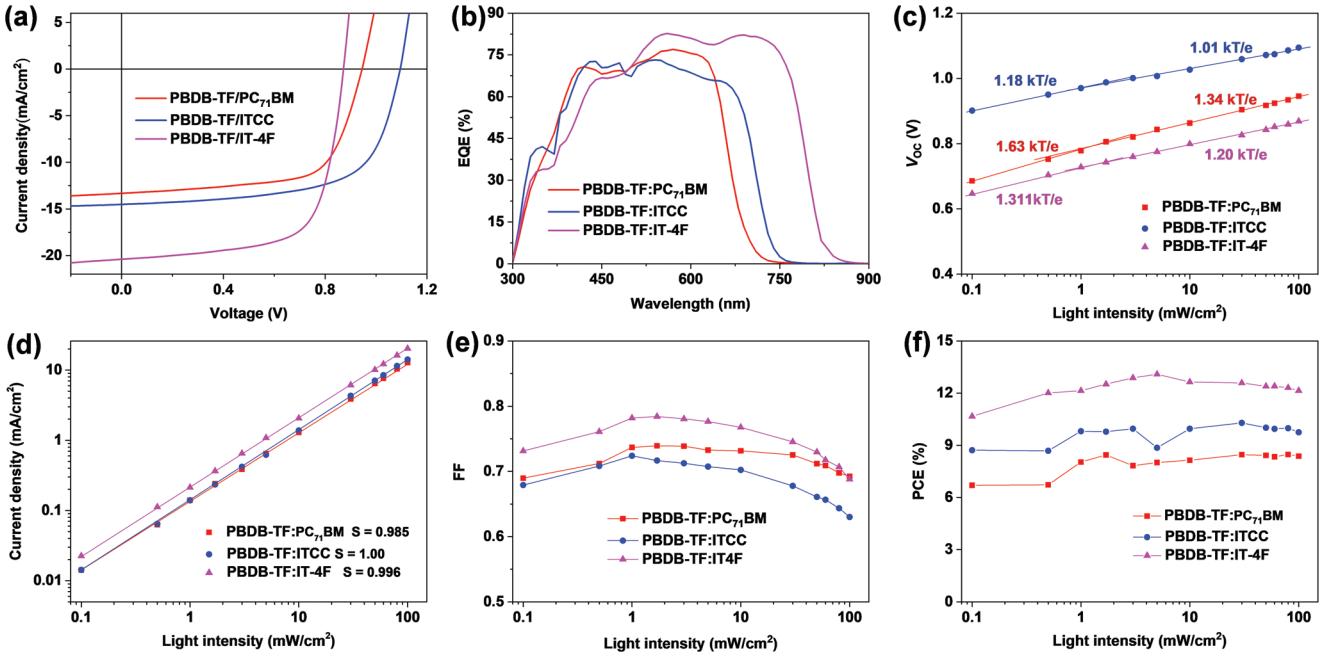

Figure 3. a) *J–V* curves of the three OPV cells under global AM 1.5 G illumination. b) EQE spectra of the devices. c–f) The change of photovoltaic parameters on varied solar illumination intensities from 0.1 to 100 mW cm^{-2}, V_{OC}, J_{SC}, FF, and PCE.

thiophene groups. Compared with IT-4F, the reduced intramolecular transfer effect in ITCC leads to its blueshifted absorption and upshifted EA, making it more suitable for indoor applications. Although the PBDB-TF:ITCC combination may not have a higher PCE than PBDB-TF:IT-4F in the OPV cells under AM 1.5 G illumination, it is more likely to obtain higher performance than the PBDB-TF:IT-4F combination in the indoor light environment.

Because photovoltaic cells have low carrier density under weak light environment, the increased resistance resulted from increasing area will not be the dominated reason in affecting the large-area device performance.[31,32] We fabricated the 1 cm^2 OPV cells using a device structure of ITO substrate/poly(3,4-ethylene-dioxythiophene):(styrene sulfonate) (PEDOT:PSS)/active layer/poly[(9,9-bis(3′-((*N*,*N*-dimethyl)-*N*-ethylammonium)-propyl)-2,7-fluorene)-*alt*-2,7-(9,9-dioctylfluorene)] (PFN-Br)/Al to study the photovoltaic performance of the donor:acceptor blends, where the PEDOT:PSS and PFN-Br worked as anode and cathode interlayers, respectively. We optimized the donor:acceptor ratio, solvent additive content, and the thermal annealing to get the best PCEs. As a contrast, we first investigated the photovoltaic performance of the OPV cells under AM 1.5 G illumination. The detailed device parameters deduced from the *J–V* characteristics (**Figure 3**a) are collected in **Table 1**. The PBDB-TF:IT-4F-based OPV cell yields the best PCE of 12.2%, with a V_{OC} of 0.872 V, a J_{SC} of 20.4 mA cm^{-2}, and an FF of 0.687. When IT-4F is replaced by ITCC, the V_{OC} of the OPV cell increases significantly to 1.10 V, while the J_{SC} drops to 14.5 mA cm^{-2}, resulting in a PCE of 10.3%. For the PBDB-TF:PC$_{71}$BM-based device, a moderate V_{OC} of 0.945 V is recorded. The corresponding J_{SC} and FF are 13.3 mA cm^{-2} and 0.671, respectively, leading to an overall PCE of 8.43%. By linearly increasing voltage (photo-CELIV) measurements[33] in Figure S3 (Supporting Information), the mobilities of the faster carrier component are estimated as 1.69×10^{-4} cm^2 V^{-1} s^{-1} for PBDB-TF:PC$_{71}$BM, 3.82×10^{-4} cm^2 V^{-1} s^{-1} for PBDB-TF:ITCC, and 6.31×10^{-5} cm^2 V^{-1} s^{-1} for PBDB-TF:IT-4F, respectively.

Figure 3b shows the external quantum efficiencies (EQEs) of the OPV cells. The calculated integrated current densities have a good consistency with the *J–V* characterizations (Table 1). The broad photoresponse range and high EQE values for the PBDB-TF:IT-4F-based device agree with its measured J_{SC} under 1 sun illumination. What should be noted is that the EQE in the range of 700–800 nm makes a great contribution to the current density. However, under indoor light source illumination (Figure 1b), there is almost no current density converted from this range. The gradually blueshifted EQE response ranges for the PBDB-TF:ITCC and PBDB-TF:PC$_{71}$BM devices should be

Table 1. Detailed photovoltaic parameters of the OPV cells under AM 1.5 G illumination.

Device	V_{OC} [V]	J_{SC} [mA cm^{-2}]	J_{cal}[a)] [mA cm^{-2}]	FF	PCE[b)] [%]	E_g [eV]	E_{loss} [eV]
PBDB-TF:PC$_{71}$BM	0.945	13.3	12.9	0.671	8.43 (8.21 ± 0.16)	1.87	0.925
PBDB-TF:ITCC	1.10	14.5	14.3	0.643	10.3 (9.98 ± 0.18)	1.75	0.650
PBDB-TF:IT-4F	0.872	20.4	20.1	0.687	12.2 (11.9 ± 0.20)	1.57	0.698

[a)] J_{cal} is calculated by EQE curve; [b)] The average parameters were calculated from more than 20 independent cells.

partially responsible for the decreased current densities under 1 sun illumination, but will match better with the spectra of indoor light sources. However, for the PBDB-TF:$PC_{71}BM$ device, energy loss (E_{loss}) is as large as 0.925 eV when referring to the derivative of the EQE edge (Figure S4, Supporting Information),[34] which is much higher than the other two nonfullerene acceptor-based OPV cells (0.650 eV for ITCC device and 0.698 eV for IT-4F device).

Indoor environments usually have light intensities around 100–1000 lux, which are only ≈0.1%–1% of the standard solar emission intensity.[35,36] Therefore, we studied the photovoltaic performance of the three OPV cells under different solar light intensities. Figure 3c,d shows the changes of V_{OC} and J_{SC} on light intensity at logarithmic forms. As shown in Figure 3c, when the light intensity decreased from 100 to 0.1 mW cm^{-2}, the three OPV cells show a varied decrease of V_{OC}. Among which, the PBDB-TF:ITCC-based OPV cell shows the minimum V_{OC} decrease of 18.1%, which is much smaller than the other devices (over 25% decrease). The fitted slopes at weak light intensities (<1 mW cm^{-2}) are higher than that at strong light conditions (>1 mW cm^{-2}), implying the trap-assisted recombination processes enhance at weak light intensities. By fitting the curves of J_{SC} versus light intensity, slopes of ≈1 are observed, suggesting the bimolecular recombination is weak in these devices (Figure 3d).[37] As the light intensity weakens, the FF first shows the first increase and then a decreasing trend (Figure 3e). The initial increase of FF should be ascribed to the decreased charge carrier density with weakened light intensities, while the reverse trend at the weak light intensity region is observed. As shown in Figure S5 (Supporting Information), we measured *J*–*V* curves in the dark, from which shunt resistance of all the device can be calculated as ≈8×10^5 Ω cm^{-2}. The lower shunt resistance may be the reason for the decay at weak light intensities.[38,39] The PBDB-TF:ITCC- and PBDB-TF:IT-4F-based OPV cells display a much greater increase of FF at 0.1 mW cm^{-2} than that at 100 mW cm^{-2}, while the PBDB-TF:$PC_{71}BM$ devices show very close FF at the different light intensities of 0.1 and 100 mW cm^{-2}. The change of PCE on light intensity is shown in Figure 3f.

It should be noted that the illumination intensities of the weak light sources are of great importance in determining the PCEs of the photovoltaic cells, which should be measured accurately. Under standard AM 1.5G condition, photovoltaic results were recorded using standard light sources. The corresponding light intensity was also accurately calibrated through the standard cell. However, an accurate evaluation of performance was absent under indoor light conditions when low-precision lux meters, such as a LX-1330B, were used to evaluate the light intensities, which lead to large errors. Although the emission spectra of the light source were provided commonly, it was not carefully evaluated how much integral current could be obtained in theory to verify the accuracy of the results.[40–42]

Here, we used a high-precision fiber optics spectrometer (Maya2000 Pro, Ocean Optics) to evaluate the light intensities. Common FL and LED lamps were employed as light source to simulate the indoor light environment. As an example, photovoltaic performance is investigated in detail by employing a warm white LED lamp (2700 K). As shown in **Figure 4**a, the illumination intensity of LED lamp (2700 K) varied at 200, 500, and 1000 lux, with the total integrated power in the whole spectral region calculated as 60.4, 151.1, and 302.2 μW cm^{-2}, respectively. By combining the photon flux spectrum with its corresponding illumination intensity, a theoretically integral current can be obtained. The details of the theoretical calculation for

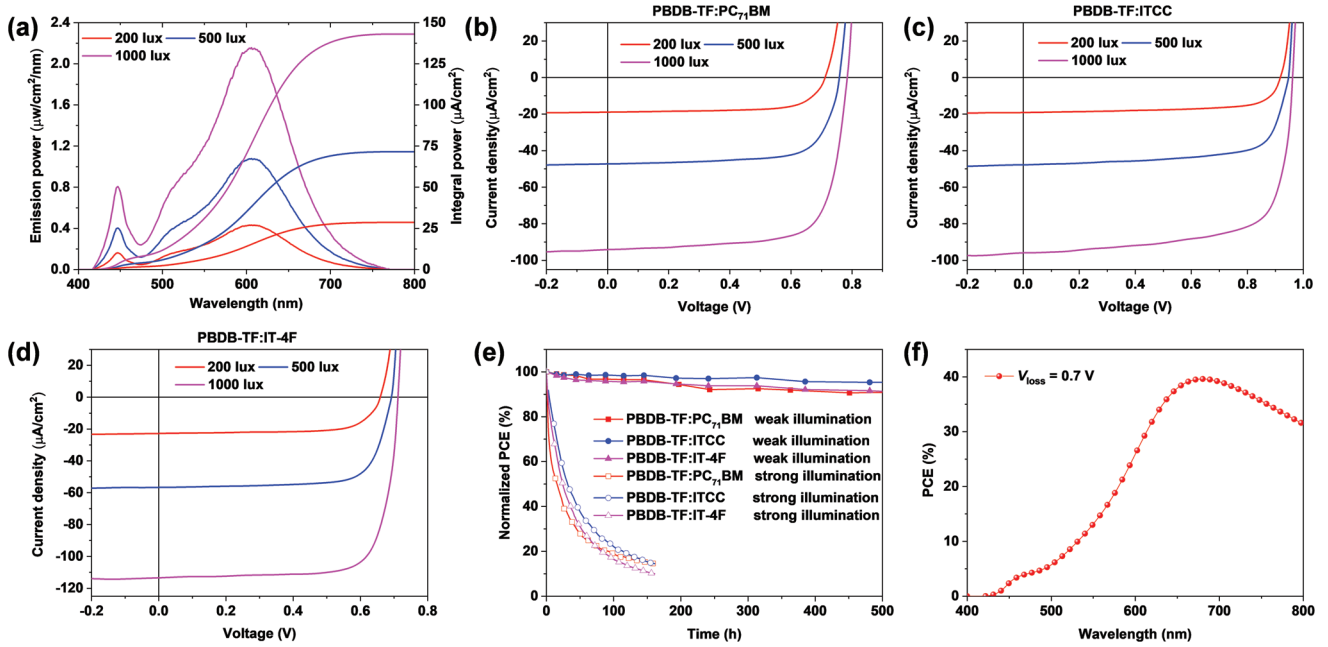

Figure 4. a) Emission power and integral current density spectra of the warm white LED, 2700 K. b–d) *J*–*V* characterizations of the PBDB-TF:$PC_{71}BM$-based (b), PBDB-TF:ITCC-based (c), and PBDB-TF:IT-4F-based (d) OPV cells under warm white LED (2700 K) illumination with varied light intensities of 200, 500, and 1000 lux. e) The stability of the three OPV cells under continuous illumination of weak and strong light. f) Efficiency prediction of OPV cells for indoor application.

Table 2. The photovoltaic parameters of the OPV cells under different light sources with different light intensities.

Device/light sources	Pin [uW cm^{-2}]	V_{OC} [V]	J_{SC} (μA cm^{-2}]	FF	Pout [uW cm^{-2}]	Intensity [lux]	PCE[a)] [%]
PBDB-TF:$PC_{71}BM$/LED 2700 K	60.4	0.712	18.9	0.713	9.59	200	15.9 (14.8 ± 0.5)
	151.1	0.758	47.2	0.727	26.0	500	17.2 (16.5 ± 0.5)
	302.2	0.784	94.1	0.741	54.7	1000	18.1 (17.4 ± 0.4)
PBDB-TF:IT-4F/LED 2700 K	60.4	0.659	22.8	0.734	11.0	200	18.2 (17.5 ± 0.4)
	151.1	0.692	56.6	0.756	29.6	500	19.6 (19.0 ± 0.4)
	302.2	0.712	113.0	0.780	62.8	1000	20.8 (20.4 ± 0.3)
PBDB-TF:ITCC/LED 2700 K	60.4	0.918	19.2	0.700	12.3	200	20.4 (19.5 ± 0.6)
	151.1	0.948	47.8	0.706	32.0	500	21.2 (20.5 ± 0.5)
	302.2	0.962	95.8	0.722	66.5	1000	22.0 (21.3 ± 0.4)
LED 6500 K	159.0	0.949	48.5	0.703	32.4	500	20.4 (19.9 ± 0.3)
FL 2700 K	124.0	0.944	39.5	0.731	27.3	500	22.0 (20.0 ± 0.7)
FL 6500 K	154.7	0.945	45.9	0.745	32.3	500	20.9 (19.8 ± 0.7)

[a)]The average parameters were calculated from more than 20 independent cells.

integral current densities are provided in the Supporting Information ("Calculations" section). As provided in Figure 4a, at 200, 500, and 1000 lux, the theoretically integral current density is calculated as 28.6, 71.5, and 143.1 μA cm^{-2}, respectively.

Figure 4b–d shows the *J*–*V* characterizations of the three devices; the detailed photovoltaic parameters are collected in **Table 2**. With the increase of the light intensities from 200 to 1000 lux, the OPV cells show significantly increased J_{SC} and V_{OC} due to the increased input photon number. As all of the devices can effectively utilize the LED light, the J_{SC} values of each of the OPV cells at the same light intensity do not show as many differences as when under 1 sun illumination. For example, under a light intensity of 200 lux, the three devices show close J_{SC} values of around 20 μA cm^{-2}. When the light intensity increases to 1000 lux, J_{SC} values of around 100 μA cm^{-2} are recorded for the OPV cells. For the three devices, the fitting slope of J_{SC} versus light intensity is ≈1, which implies that the ratio of photons to electrons remains constant with the decrease of light intensity. Therefore, the EQE curve can be used to evaluate the accuracy of indoor measurements. At 500 lux, based on the EQE and photon flux spectrum, the integral current densities of the cells are calculated to be 47.0 μA cm^{-2} for PBDB-TF:$PC_{71}BM$, 47.6 μA cm^{-2} for PBDB-TF:ITCC, and 56.1 μA cm^{-2} for PBDB-TF:IT-4F, respectively, confirming the reliability of *J*–*V* measurement.

For the V_{OC}, clear increases are also observed in all of the OPV cells with the increase of light intensities from 200 to 1000 lux. In comparison with the results obtained under 1 sun illumination, the PBDB-TF:ITCC-based device shows the smallest V_{OC} decrease when compared to the other two devices. For instance, at a light intensity of 500 lux, the PBDB-TF:ITCC-based OPV cell yields a V_{OC} of 0.948 V, corresponding to a V_{OC} decrease of 0.152 V. By contrast, at the same light intensity, the V_{OC} decreases are 0.187 and 0.180 V for the PBDB-TF:$PC_{71}BM$ and PBDB-TF:IT-4F-based OPV cells, respectively. This advantage seen from the PBDB-TF:ITCC-based device will contribute greatly to its high PCEs in indoor light environments.

When the light intensity increases from 200 to 1000 lux, the FFs are also improved slightly to over 0.7. Impressively, the PBDB-TF:IT-4F yields an FF of 0.78 at a light intensity of 1000 lux. This trend is similar to the phenomenon observed in the weak light intensity region for the OPV cells measured under sunlight illumination. Overall, gradually increased PCEs are achieved with the increase of light intensities. Due to the advantage of V_{OC}, the PBDB-TF:ITCC-based device obtains superior photovoltaic performance than PBDB-TF:IT-4F-based device at the same illumination conditions. At an illumination of 1000 lux, the PBDB-TF:ITCC-based OPV cell shows the maximum PCE of 22.0% with a V_{OC} of 0.962 V, a J_{SC} of 95.8 μA cm^{-2}, and an FF of 0.722. The PBDB-TF:IT-4F-based device also yields a PCE of over 20%. In contrast, the PBDB-TF:$PC_{71}BM$-based device obtains the lowest PCE of 18.1% under the same conditions. For the optimal device based on PBDB-TF:ITCC, the photovoltaic results using other LED and FL lamps are provided in Figure S6 (Supporting Information) and Table 2. High performance of PBDB-TF:ITCC-based device is mainly attributed to matching absorption spectrum, low V_{loss}, high EQE, and low charge recombination.

Furthermore, we measured the device stability under continuous illumination at different light intensities in the air (Figure 4e). Here, the devices were completely encapsulated by glass with an epoxy adhesive to block water and oxygen. Under weak illumination conditions (the 2700 K LED), device performance was tested with a temperature of ≈25–30°C. Under strong illumination conditions, device performance was measured by utilizing a white LED, with the corresponding emission spectrum provided in Figure S7 (Supporting Information). Due to the continuous and strong illumination conditions, the devices were naturally heated to ≈45 °C. Impressively, the three devices under weak light intensity showed much better stability over a long time, with over 90% of the original PCE obtained. However, all three of the devices suffer a fast decrease of PCEs under strong light, as seen in Figure 4e. After 160 h, only <15% of the original PCEs are recorded. The good device stability of

the OPV cells under indoor light illumination is a very good feature for practical applications. In addition, the continuous thermal stability (≈45 °C) was also investigated in the dark. As shown in Figure S8 (Supporting Information), the PCEs of the three devices decrease significantly after 160 h; the decay trend is lower than that under strong irradiation conditions. These results demonstrate that strong illumination and heat are two main factors for the decay of OPV device performance. As the indoor OPV cells are working at low power conditions and mild environments with mild temperatures and humidity, device stability is more dependent on the intrinsic blend morphology and interface. But, AM 1.5G solar light produces strong illumination and heat so as to potentially increase molecular disorder and possibly induce the photodegradation of organic material,[43,44] which is an obstacle to the application for organic photovoltaic cells. Furthermore, we find that the PBDB-TF:ITCC-based OPV cell shows slightly better stability compared to other cells under the same conditions. This phenomenon may be associated with the detailed molecular structures, and more efforts are needed to get a deeper understanding in future research.

Overall, although we have demonstrated an excellent photovoltaic result for indoor light applications in the field of OPV cells, it is worth noting that the photoresponse of the PBDB-TF:ITCC-based OPV cell still does not match particularly well with the large E_{loss}. Therefore, we believe that there is much room for improvement in performance for indoor applications. In OPV cells, E_{loss} values of 0.50–0.60 eV have been obtained under AM 1.5G conditions.[45,46] Generally, V_{OC} is directly correlated with Gaussian density of states affected by light illumination, and the decreases of light intensity will reduce the V_{OC}.[47] Considering an extra voltage loss of ≈0.15 V under indoor conditions compared with the AM 1.5G conditions,[31,48] we set V_{loss} as 0.7 V. The EQE can be set to 90% due to similar values found in OPV cells.[49] In general, the organic device shows an enhanced FF under weak light and, thus, has the potential to achieve an ideal FF.[39] Figure S9 (Supporting Information) shows the curves of the FF based on the empirical relationship. As the prediction results show in Figure 4f, the calculated, theoretical limit of PCE is 40% at a bandgap of 1.82 eV under LED (2700K). The calculation scheme is provided in the Supporting Information ("Calculations" section). The comparison of these results with the AM 1.5 G is extremely striking. Therefore, OPV cells can be expected for indoor application in the future.

To conclude, we study the applications of OPV cells in an indoor light environment. A wide-bandgap combination of a polymer donor PBDB-TF and a nonfullerene acceptor ITCC was used as the photoactive layer in the OPV cell to make a good match with the emission spectrum of a warm white LED light. With the advantage of low photovoltage decrease at weak light intensities, the PBDB-TF:ITCC-based device yields top PCEs of over 20% at 200, 500, and 1000 lux LED illuminations at a photoactive area of 1 cm^2. When the acceptor ITCC was replaced by the low-bandgap acceptor IT-4F with superior performance under 1 sun illumination, the broad absorption beyond 700 nm will almost not contribute to the current density and, on the contrary, generate its low photovoltage. We also explored the application of PBDB-TF:PC_{71}BM-based devices in indoor light. Although it has a well-matched spectrum with the LED illumination, the large photovoltage decrease results in its relatively low PCEs. Our work presents the good applications of OPV cells in indoor light environments; better performance can be expected by using wide-bandgap photoactive materials with low V_{loss}.

Supporting Information

Supporting Information is available from the Wiley Online Library or from the author.

Acknowledgements

J.H. would like to acknowledge financial support from the National Natural Science Foundation of China (Grant Nos. 21835006, 91633301, and 51673201), Beijing National Laboratory for Molecular Sciences (BNLMS-CXXM-201903), and the Chinese Academy of Sciences (Grant Nos. XDB12030200). H.Y. acknowledges financial support from the National Natural Science Foundation of China (Grant No. 21805287) and the Youth Innovation Promotion Association CAS (Grant No. 2018043).

Conflict of Interest

The authors declare no conflict of interest.

Keywords

indoor application, organic photovoltaic cells, photostability, power conversion efficiency

Received: July 14, 2019
Revised: August 10, 2019
Published online: September 6, 2019

[1] G. Xu, L. Shen, C. Cui, S. Wen, R. Xue, W. Chen, H. Chen, J. Zhang, H. Li, Y. Li, Y. Li, *Adv. Funct. Mater.* **2017**, *27*, 1605908.
[2] L. Wen, Q. Chen, F. Sun, S. Song, L. Jin, Y. Yu, *Sci. Rep.* **2015**, *4*, 7036.
[3] K.-S. Chen, J.-F. Salinas, H.-L. Yip, L. Huo, J. Hou, A. K. Y. Jen, *Energy Environ. Sci.* **2012**, *5*, 9551.
[4] F. Liu, Z. Zhou, C. Zhang, J. Zhang, Q. Hu, T. Vergote, F. Liu, T. P. Russell, X. Zhu, *Adv. Mater.* **2017**, *29*, 1606574.
[5] Y. Zhou, C. Fuentes-Hernandez, T. M. Khan, J. C. Liu, J. Hsu, J. W. Shim, A. Dindar, J. P. Youngblood, R. J. Moon, B. Kippelen, *Sci. Rep.* **2013**, *3*, 1536.
[6] M. Kaltenbrunner, M. S. White, E. D. Glowacki, T. Sekitani, T. Someya, N. S. Sariciftci, S. Bauer, *Nat. Commun.* **2012**, *3*, 770.
[7] J. Hou, O. Inganas, R. H. Friend, F. Gao, *Nat. Mater.* **2018**, *17*, 119.
[8] C. Duan, K. Zhang, C. Zhong, F. Huang, Y. Cao, *Chem. Soc. Rev.* **2013**, *42*, 9071.
[9] P. Cheng, G. Li, X. Zhan, Y. Yang, *Nat. Photonics* **2018**, *12*, 131.
[10] C. Dou, J. Liu, L. Wang, *Sci. China: Chem.* **2017**, *60*, 450.
[11] Y. Liu, C. Zhang, D. Hao, Z. Zhang, L. Wu, M. Li, S. Feng, X. Xu, F. Liu, X. Chen, Z. Bo, *Chem. Mater.* **2018**, *30*, 4307.
[12] C. Lee, H. Kang, W. Lee, T. Kim, K. H. Kim, H. Y. Woo, C. Wang, B. J. Kim, *Adv. Mater.* **2015**, *27*, 2466.
[13] L. Dou, J. You, Z. Hong, Z. Xu, G. Li, R. A. Street, Y. Yang, *Adv. Mater.* **2013**, *25*, 6642.

[14] H. W. Lin, S. W. Chiu, L. Y. Lin, Z. Y. Hung, Y. H. Chen, F. Lin, K. T. Wong, *Adv. Mater.* **2012**, *24*, 2269.
[15] J. Kong, I. W. Hwang, K. Lee, *Adv. Mater.* **2014**, *26*, 6275.
[16] J. D. Servaites, M. A. Ratner, T. J. Marks, *Energy Environ. Sci.* **2011**, *4*, 4410.
[17] H. Yao, D. Qian, H. Zhang, Y. Qin, B. Xu, Y. Cui, R. Yu, F. Gao, J. Hou, *Chin. J. Chem.* **2018**, *36*, 491.
[18] S. M. Menke, N. A. Ran, G. C. Bazan, R. H. Friend, *Joule* **2018**, *2*, 25.
[19] Y. Cui, H. Yao, J. Zhang, T. Zhang, Y. Wang, L. Hong, K. Xian, B. Xu, S. Zhang, J. Peng, Z. Wei, F. Gao, J. Hou, *Nat. Commun.* **2019**, *10*, 2515.
[20] B. Fan, D. Zhang, M. Li, W. Zhong, Z. Zeng, L. Ying, F. Huang, Y. Cao, *Sci. China: Chem.* **2019**, *62*, 746.
[21] H. Kang, G. Kim, J. Kim, S. Kwon, H. Kim, K. Lee, *Adv. Mater.* **2016**, *28*, 7821.
[22] B. Minnaert, P. Veelaert, *Thin Solid Films* **2011**, *519*, 7537.
[23] M. C. Scharber, D. Mühlbacher, M. Koppe, P. Denk, C. Waldauf, A. J. Heeger, C. J. Brabec, *Adv. Mater.* **2006**, *18*, 789.
[24] W. Li, L. Ye, S. Li, H. Yao, H. Ade, J. Hou, *Adv. Mater.* **2018**, *30*, 1707170.
[25] W. Shockley, W. T. Read, *Phys. Rev.* **1952**, *87*, 835.
[26] S. R. Cowan, A. Roy, A. J. Heeger, *Phys. Rev. B* **2010**, *82*, 245207.
[27] V. Gupta, A. K. Kyaw, D. H. Wang, S. Chand, G. C. Bazan, A. J. Heeger, *Sci. Rep.* **2013**, *3*, 1965.
[28] M. Zhang, X. Guo, W. Ma, H. Ade, J. Hou, *Adv. Mater.* **2015**, *27*, 4655.
[29] J. Yuan, Y. Zhang, L. Zhou, G. Zhang, H.-L. Yip, T.-K. Lau, X. Lu, C. Zhu, H. Peng, P. A. Johnson, M. Leclerc, Y. Cao, J. Ulanski, Y. Li, Y. Zou, *Joule* **2019**, *3*, 1.
[30] H. Yao, L. Ye, J. Hou, B. Jang, G. Han, Y. Cui, G. M. Su, C. Wang, B. Gao, R. Yu, H. Zhang, Y. Yi, H. Y. Woo, H. Ade, J. Hou, *Adv. Mater.* **2017**, *29*, 1700254.
[31] H. K. H. Lee, Z. Li, J. R. Durrant, W. C. Tsoi, *Appl. Phys. Lett.* **2016**, *108*, 253301.
[32] R. Steim, T. Ameri, P. Schilinsky, C. Waldauf, G. Dennler, M. Scharber, C. J. Brabec, *Sol. Energy Mater. Sol. Cells* **2011**, *95*, 3256.
[33] M. Stephen, K. Genevičius, G. Juška, K. Arlauskas, R. C. Hiorns, *Polym. Int.* **2017**, *66*, 13.
[34] Y. M. Wang, D. P. Qian, Y. Cui, H. T. Zhang, J. H. Hou, K. Vandewal, T. Kirchartz, F. Gao, *Adv. Energy Mater.* **2018**, *8*, 1801352.
[35] B. Minnaert, P. Veelaert, *Energies* **2014**, *7*, 1500.
[36] M. Freitag, J. Teuscher, Y. Saygili, X. Zhang, F. Giordano, P. Liska, J. Hua, S. M. Zakeeruddin, J.-E. Moser, M. Grätzel, A. Hagfeldt, *Nat. Photonics* **2017**, *11*, 372.
[37] A. K. K. Kyaw, D. H. Wang, V. Gupta, W. L. Leong, L. Ke, G. C. Bazan, A. J. Heeger, *ACS Nano* **2013**, *7*, 4569.
[38] Y. Zhou, T. M. Khan, J. W. Shim, A. Dindar, C. Fuentes-Hernandez, B. Kippelen, *J. Mater. Chem. A* **2014**, *2*, 3492.
[39] M. A. Green, *Solid-State Electron.* **1981**, *24*, 788.
[40] H. K. H. Lee, J. Wu, J. Barbé, S. M. Jain, S. Wood, E. M. Speller, Z. Li, F. A. Castro, J. R. Durrant, W. C. Tsoi, *J. Mater. Chem. A* **2018**, *6*, 5618.
[41] H. K. H. Lee, J. Barbé, S. M. P. Meroni, T. Du, C.-T. Lin, A. Pockett, J. Troughton, S. M. Jain, F. De Rossi, J. Baker, M. J. Carnie, M. A. McLachlan, T. M. Watson, J. R. Durrant, W. C. Tsoi, *Sol. RRL* **2019**, *3*, 1800207.
[42] H. Yin, J. K. W. Ho, S. H. Cheung, R. J. Yan, K. L. Chiu, X. T. Hao, S. K. So, *J. Mater. Chem. A* **2018**, *6*, 8579.
[43] X. Du, T. Heumueller, W. Gruber, A. Classen, T. Unruh, N. Li, C. J. Brabec, *Joule* **2019**, *3*, 215.
[44] C. H. Peters, I. T. Sachs-Quintana, W. R. Mateker, T. Heumueller, J. Rivnay, R. Noriega, Z. M. Beiley, E. T. Hoke, A. Salleo, M. D. McGehee, *Adv. Mater.* **2012**, *24*, 663.
[45] X. Xu, T. Yu, Z. Bi, W. Ma, Y. Li, Q. Peng, *Adv. Mater.* **2018**, *30*, 1703973.
[46] D. Baran, T. Kirchartz, S. Wheeler, S. Dimitrov, M. Abdelsamie, J. Gorman, R. S. Ashraf, S. Holliday, A. Wadsworth, N. Gasparini, P. Kaienburg, H. Yan, A. Amassian, C. J. Brabec, J. R. Durrant, I. McCulloch, *Energy Environ. Sci.* **2016**, *9*, 3783.
[47] N. K. Elumalai, A. Uddin, *Energy Environ. Sci.* **2016**, *9*, 391.
[48] B. P. Lechêne, M. Cowell, A. Pierre, J. W. Evans, P. K. Wright, A. C. Arias, *Nano Energy* **2016**, *26*, 631.
[49] J. Zhao, Y. Li, G. Yang, K. Jiang, H. Lin, H. Ade, W. Ma, H. Yan, *Nat. Energy* **2016**, *1*, 15027.

